5. Gu, Y., Rosenblatt, J. & Morgan, D. O. *EMBO J.* **11,** 3995–4005 (1992).
6. Desai, D., Gu, Y. & Morgan, D. O. *Molec. Biol. Cell* **3,** 571–582 (1992).
7. Ducommun, B. *et al. EMBO J.* **10,** 3311–3319 (1991).
8. Gould, K. L., Moreno, S., Owen, D. J., Sazer, S. & Nurse, P. *EMBO J.* **10,** 3297–3309 (1991).
9. Solomon, M. J., Lee, T. & Kirschner, M. W. *Molec. Biol. Cell* **3,** 13–27 (1992).
10. Shuttleworth, J., Godfrey, R. & Colman, A. *EMBO J.* **9,** 3233–3240 (1990).
11. Fesquet, D. *et al. EMBO J.* **12,** 3111–3121 (1993).
12. Poon, R. Y., Yamashita, K., Adamczewski, J. P., Hunt, T. & Shuttleworth, J. *EMBO J.* **12,** 3123–3132 (1993).
13. Solomon, M. J., Harper, J. W. & Shuttleworth, J. *EMBO J.* **12,** 3133–3142 (1993).
14. Fields, S. & Song, O. *Nature* **340,** 245–246 (1989).
15. Gyuris, J., Golemis, E., Chertkov, H. & Brent, R. *Cell* **75,** 791–803 (1993).
16. Molz, L. & Beach, D. *EMBO J.* **12,** 1723–1732 (1993).
17. Valay, J. G., Simon, M. & Faye, G. *J. molec. Biol.* **234,** 307–310 (1993).
18. Lew, D. J., Dulic, V. & Reed, S. I. *Cell* **66,** 1197–1206 (1991).
19. Connell-Crowley, L., Solomon, M. J., Wei, N. & Harper, J. W. *Molec. Biol. Cell* **4,** 79–92 (1993).
20. Tassan, J.-P., Schultz, S., Bartek, J. & Nigg, E. A. *J. cell. Biol.* (in the press).
21. Devereux, J., Haeberli, P. & Smithies, O. *Nucleic Acids Res.* **12,** 387–395 (1984).
22. Levedakou, E. N. *et al. Oncogene* **9,** 1977–1988 (1994).
23. Hinds, P. W. *et al. Cell* **70,** 993–1006 (1992).
24. Harlow, E. & Lane, D. *Antibodies: A Laboratory Manual* (Cold Spring Harbor Laboratory, Cold Spring Harbor, 1988).
25. Ortiz, M. L., Calero, M., Patron, C. F., Castellanos, L. & Mendez, E. *FEBS Lett.* **296,** 300–304 (1992).
26. Schägger, H. & von Jagow, G. *Analyt. Biochem.* **166,** 368–379 (1987).

ACKNOWLEDGEMENTS. We thank R. Finley and R. Brent for interaction trap reagents; the Harlow laboratory for the GST-cdk2 plasmid; D. Morgan for cyclin A baculovirus; and members of the Weinberg laboratory, especially C. Sardet and R. Medema, for reagents, help and discussion. This work was supported by a grant from the American Cancer Society to R.A.W., T.P.M. is a recipient of a Human Frontiers Science Program Organisation long-term fellowship; J.-P.T. holds a postdoctoral fellowship from the French Cancer League; S.F. and G.J.H. are supported by the Swiss NSF and E.A.N. by the Swiss NSF and the Swiss Cancer League. R.A.W. is an American Cancer Society Research Professor. The GenBank accession number for the cyclin H cDNA sequence is U11791.

p15^{INK4B} is a potential effector of TGF-β-induced cell cycle arrest

Gregory J. Hannon & David Beach*

Howard Hughes Medical Institute, Cold Spring Harbor Laboratory, Cold Spring Harbor, New York 11724, USA

TRANSFORMING growth factor-beta (TGF-β) inhibits cell proliferation by inducing a G1-phase cell cycle arrest[1]. Normal progression through G1 is promoted by the activity of the cyclin-dependent protein kinases CDK4 and CDK6 (ref. 2), which are inhibited by the protein p16^{INK4}. We have isolated a new member of the p16^{INK4} family, p15^{INK4B}. p15 expression is induced ~30-fold in human keratinocytes by treatment with TGF-β, suggesting that p15 may act as an effector of TGF-β-mediated cell cycle arrest. The gene encoding p15 is located on chromosome 9 adjacent to the p16 gene at a frequent site of chromosomal abnormality in human tumours (9p21).

TGF-β is a multifunctional polypeptide that elicits different responses in different cell types and is the prototype of a family of growth factors, differentiation factors and morphogens[1]. For most cell types (such as epithelial, endothelial, myeloid and lymphoid) TGF-β is a negative growth factor. Exposure causes cells to cease proliferation and undergo cell cycle arrest in G1 phase[1]. Current models suggest that during G1, cyclin-dependent kinases (particularly the cyclin D-associated kinases-CDK4 and CDK6) phosphorylate the product of the retinoblastoma-susceptibility gene, *Rb*, and thus release cells from its growth inhibitory effects[2–4]. TGF-β treatment causes accumulation of Rb in the underphosphorylated state, and expression of Rb-inactivating viral oncoproteins prevents TGF-β-induced cell cycle arrest[5,6]. These results suggested that TGF-β might function by suppressing Rb phosphorylation and pointed to the possibility that one result of TGF-β treatment might be inhibition of cyclin-dependent kinases.

To investigate the mechanism by which TGF-β inhibits cell proliferation, we examined α-CDK immunoprecipitates from human keratinocytes which had been arrested in G1 by exposure to TGF-β[7,8]. Immunoprecipitates of two G1-specific cyclin kinases, CDK4 and CDK6, contained several associated proteins of low molecular weight (Fig. 1*c*). These included p16^{INK4}, a previously characterized CDK4 inhibitor[9], and two additional proteins of relative molecular mass (M_r) ~15,000 and ~15,500. These proteins were not recovered in parallel CDC2 or CDK2 immunoprecipitates (not shown) but were recovered (albeit to a low extent) in α-p16 immunoprecipitates (Fig. 1*c*), suggesting that p15, p15.5 and p16 might be related. This was confirmed by western blotting of CDK4 and CDK6 immunoprecipitates which demonstrated that p15 and p15.5 were weakly cross reactive with the p16 antiserum (not shown).

To isolate clones encoding putative p16 relatives, we constructed a cDNA library from TGF-β arrested HaCaT cells and probed this library at low stringency with the p16 coding sequence. One clone obtained in this screen encoded a protein of 137 amino acids (predicted M_r 14,700 (14.7K) with homology to p16^{INK4}. On the basis of this homology and the biochemical properties described below, we have named this protein p15^{INK4B} (inhibitor of CDK4-B). The first 50 amino-acid residues of p15 and p16 share ~44% identity (Fig. 1*b*). This is followed by an 81 amino acid region of ~97% identity after which p15 and p16 diverge. The sequence of p15^{INK4B} can be divided into four ankyrin repeats suggesting that this structural motif is conserved in the INK4 family[9]. *In vitro* translation of the p15^{INK4B} cDNA produced a protein which precisely comigrated with the p15 present in CDK4, CDK6 and p16 immunoprecipitates from TGF-β-arrested HaCaT cells (not shown). Identity of these proteins was confirmed by protease and chemical cleavage mapping (Fig. 1*d*).

To investigate the functional similarity of p15 and p16, we expressed p15 as a fusion protein in bacteria and tested its ability to bind and inhibit cyclin-dependent kinases. p15^{INK4B} specifically bound CDK4 and CDK6 but did not appreciably bind CDC2, CDK2 or CDK5 (Fig. 2*a*) To assess the consequences of binding, p15 was added to active cyclin-CDK complexes expressed in insect cells. p15 specifically inhibited the cyclin D-CDK4 and cyclin D-CDK6 enzymes (Fig. 2*b*, *c*) but had no effect on CDK2-cyclin A kinase (not shown). Thus, p15^{INK4B} is a functional member of the p16^{INK4} family.

The carboxy-terminal portion of the p15 sequence was reminiscent of the amino-acid sequence predicted from a genomic locus, *MTS2*, which had been previously identified[10]. Comparison revealed that the reported *MTS2* sequence encodes the C-terminal 86 amino acids of p15^{INK4B}. *MTS2* lies adjacent to the p16 gene at 9p21, and localization of the p15 gene to this position was confirmed by FISH mapping (D. Demetrick, G.J.H. and D.B., unpublished). Although a fragment of the p15 gene has already been designated as *MTS2* (for multiple tumour suppressor 2), we favour the name *INK4B*, because it denotes a demonstrated property of the gene product.

p15^{INK4B} was first noted in immunoprecipitates from HaCaT cells which had been arrested in G1 by serum starvation and subsequent restimulation in the presence of TGF-β. By comparison, asynchronous, rapidly proliferating HaCaT cells contained considerably lower levels of p15 in CDK4 and CDK6 immunoprecipitates (Fig. 3*a*). To separate effects of TGF-β from effects of G1 arrest, asynchronous cultures were treated with TGF-β for various periods, after which patterns of CDK4- and CDK6-associated proteins were examined. Although CDK-associated p16 levels were unaffected, TGF-β treatment increased association of p15 with CDK4 and CDK6 (Fig. 3*a*). Significant increases in p15 levels were observed within 2–4 h after treatment, and peak levels were reached after 6–8 h (Fig. 3*a*). Notably, TGF-β treatment also resulted in loss of CDK6 kinase activity from HaCaT cell lysates with a time course that parallelled p15 induction (Fig. 3*b*).

* To whom correspondence should be addressed.

Northern blotting of RNA from TGF-β treated cultures revealed that increases in CDK-associated p15 reflected increased abundance of p15 mRNA (Fig. 4*a*). In 2 h following TGF-β treatment, p15 mRNA levels began to rise and reached a peak induction of ~30-fold after 6–8 h (Fig. 4*a*, *e*). In contrast, p16 mRNA levels did not vary (Fig. 4*b*, *e*).

Two other mechanisms for TGF-β-mediated cell cycle arrest have been previously proposed. In mink lung fibroblasts (Mv1Lu cells), TGF-β treatment suppressed CDK4 synthesis[11]. This was deemed causal as cells could be rendered TGF-β resistant by constitutive overexpression of CDK4. In HaCaT cells, TGF-β treatment had no effect on CDK4 protein (Fig. 3*a*) or

a

```
        10                  30                  50
GAGGACTCCGCGACGGTCCGCACCCTGCGGCCAGAGCGGCTTTGAGCTCGGCTGCTTCCG
        70                  90                 110
CGCTAGGCGCTTTTTCCCAGAAGCAATCCAGGCGCGCCCGCTGGTTCTTGAGCGCCAGGA
       130                 150                 170
AAAGCCCGGAGCTAACGACCGGCCGCTCGGCACTGCACGGGGCCCCAAGCCGCAGAAGAA
       190                 210                 230
GGACGACGGGAGGGTAATGAAGCTGAGCCCAGGTCTCCTAGGAAGGAGAGAGTGCGCCGG
       250                 270                 290
AGCAGCGTGGGAAAGAAGGGAAGAGTGTCGTTAAGTTTACGGCCAACGGTGGATTATCCG
       310                 330                 350
GGCCGCTGCGCGTCTGGGGGCTGCGGAATGCGCGAGGAGAACAAGGGCATGCCCAGTGGG
                          M  R  E  E  N  K  G  M  P  S  G
       370                 390                 410
GGCGGCAGCGATGAGGGTCTGGCCACGCCGGCGCGGGGACTAGTGGAGAAGGTGCGACAC
 G  G  S  D  E  G  L  A  T  P  A  R  G  L  V  E  K  V  R  H
       430                 450                 470
TCCTGGGAAGCCGGCGCGGATCCCAACGGAGTCAACCGTTTCGGGAGGCGCGCGATCCAG
 S  W  E  A  G  A  D  P  N  G  V  N  R  F  G  R  R  A  I  Q
       490                 510                 530
GTCATGATGATGGGCAGCGCCCGCGTGGCGGAGCTGCTGCTGCTCCACGGCGCGGAGCCC
 V  M  M  M  G  S  A  R  V  A  E  L  L  L  L  H  G  A  E  P
       550                 570                 590
AACTGCGCAGACCCTGCCACTCTCACCCGACCGGTGCATGATGCTGCCCGGGAGGGCTTC
 N  C  A  D  P  A  T  L  T  R  P  V  H  D  A  A  R  E  G  F
       610                 630                 650
CTGGACACGCTGGTGGTGCTGCACCGGGCCGGGGCGCGGCTGGACGTGCGCGATGCCTGG
 L  D  T  L  V  V  L  H  R  A  G  A  R  L  D  V  R  D  A  W
       670                 690                 710
GGTCGTCTGCCCGTGGACTTGGCCGAGGAGCGGGGCCACCGCGACGTTGCAGGGTACCTG
 G  R  L  P  V  D  L  A  E  E  R  G  H  R  D  V  A  G  Y  L
       730                 750                 770
CGCACAGCCACGGGGGACTGACGCCAGGTTCCCCAGCCGCCCACAACGACTTTATTTTCT
 R  T  A  T  G  D  *
       790                 810                 830
TACCCAATTTCCCACCCCCACCCACCTAATTCGATGAAGGCTGCCAACGGGGAGCGG
```

b

```
p15 INK4B: 1    MREENKGMPSGGGSDEGLATPA.RGLVEKVRHSWEAGADPNGVNR  44
               +  +  |   | + ||| | || ||+||   || | ||  |
p16 INK4A: 1      MDPAAGSSMEPSADWLATAAARGRVEEVRALLEAVALPNAPNS  43

p15 INK4B: 45   FGRRAIQVMMMGSARVAELLLLHGAEPNCADPATLTRPVHDAAREG  90
               +||| ||||||||||||||||||||||||||||||||||||||||
p16 INK4A: 44   YGRRPIQVMMMGSARVAELLLLHGAEPNCADPATLTRPVHDAAREG  89

p15 INK4B: 91   FLDTLVVLHRAGARLDVRDAWGRLPVDLAEERGHRDVAGYLRTATGD 137
               |||||||||||||||||||||||||||||| |||||| ||| | |
p16 INK4A  90   FLDTLVVLHRAGARLDVRDAWGRLPVDLAEELGHRDVARYLRAAAGG 136

P16 INK4A: 137  TRGSNHARIDAAEGPSDIPD                          156
```

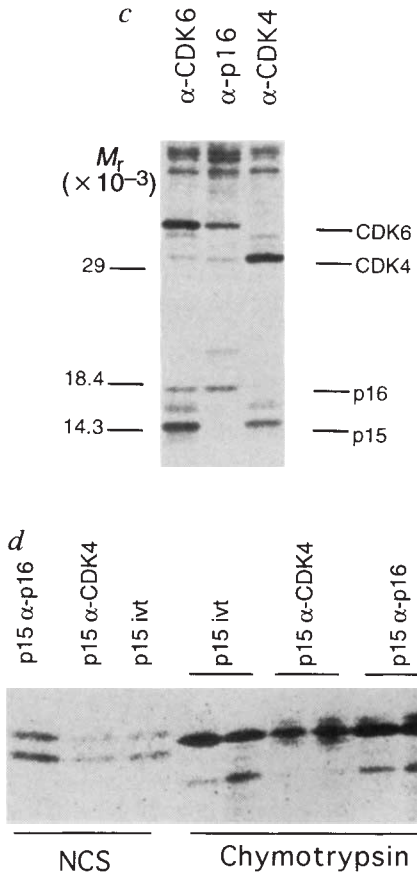

FIG. 1 Cloning of p15^{INK4B}. *a*, The sequence of the INK4B cDNA is shown along with the deduced amino-acid sequence of the INK4B protein. The underlining highlights an in-frame stop codon upstream of the presumptive initiating methionine. *b*, The deduced amino-acid sequence of p15^{INK4B} is compared with that of p16 (ref. 9). Areas of homology were identified using the BLAST program. Vertical lines indicate identity and plus signs indicate similar amino acids. The sequence of p16 has been revised from the original[9] to include eight additional amino acids at its N terminus (D. Demetrick, M. Serrano, G.J.H. and D.B., unpublished but submitted as a correction to Genbank). *c*, Immunoprecipitates of CDK4, p16 and CDK6 (as indicated) were prepared from TGF-β-arrested HaCaT cells[7,8]. Positions of CDK4, CDK6, p16 and p15 are marked. p15.5 migrates between p15 and p16 and on the basis of protease mapping could represent either a distinct protein or a modified form of p15. We note that p16 seems to bind CDK6 more effectively than CDK4 (see also Fig. 3*a*), but detailed biochemical analyses with purified components will be required to determine whether p16 indeed differs in its affinity for these proteins. The positions of labelled protein molecular weight markers, electrophoresed in parallel, are shown. Electrophoresis was carried out in a 17.5% SDS-PAGE gel. *d*, p15 was produced by *in vitro* translation (p15 ivt) or was electrophoretically purified from CDK4 (p15 α-CDK4) or p16 (p15 α-p16) immunoprecipitates such as those shown in C. Purified proteins were cleaved with *N*-chlorosuccinimide (NCS) or chymotrypsin (as indicated) before a second electrophoresis.

METHODS. HaCaT cells (a gift of P. Boukamp and N. Fusenig, German Cancer Research Center) were routinely maintained in DMEM containing 10% fetal bovine serum (FBS)[7]. For TGF-β arrest, HaCaT cells were grown to confluence in DMEM containing 10% FBS and then serum-starved for 3 days in DMEM containing 0.1% FBS. Cells were restimulated by addition of new media containing 10% FBS and 2 ng ml^{-1} TGF-β (purified from human platelets, Calbiochem). For library construction, RNA was prepared 22 h after restimulation. For the immunoprecipitations shown in *c*, cells were labelled with [^{35}S]methionine in the presence of TGF-β for 4 h beginning at 19 h after restimulation. For library construction and screening RNA was prepared from TGF-β-treated cells and from cells that were serum starved and then restimulated in the absence of TGF-β using RNAZOL B according to the manufacturer's instructions. Messenger RNA preparation and cDNA synthesis were exactly as previously described[27]. Double-stranded cDNA was ligated into λ-ZapII arms according to the manufacturers instructions. Low-stringency hybridization was performed at 50 °C in 500 mM $NaPO_4$, pH7.0, 1 mM EDTA, 15% formamide, 7% SDS, 0.1% bovine serum albumin (wash: 1 × SSC, 50 °C). The p15^{INK4B} cDNA was also isolated from a human mammary epithelial cell library provided by M. Stampfer (University of California at Berkeley). Cell lysis, immunoprecipitation and protease mapping were performed exactly as previously described[28]. For chymotrypsin digestion, either 7 µg or 1.5 µg of enzyme was used. Gels for chymotrypsin mapping contained 0.1% SDS. The CDK6 antibody was a gift of M. Meyerson (MGH, Boston)[4].

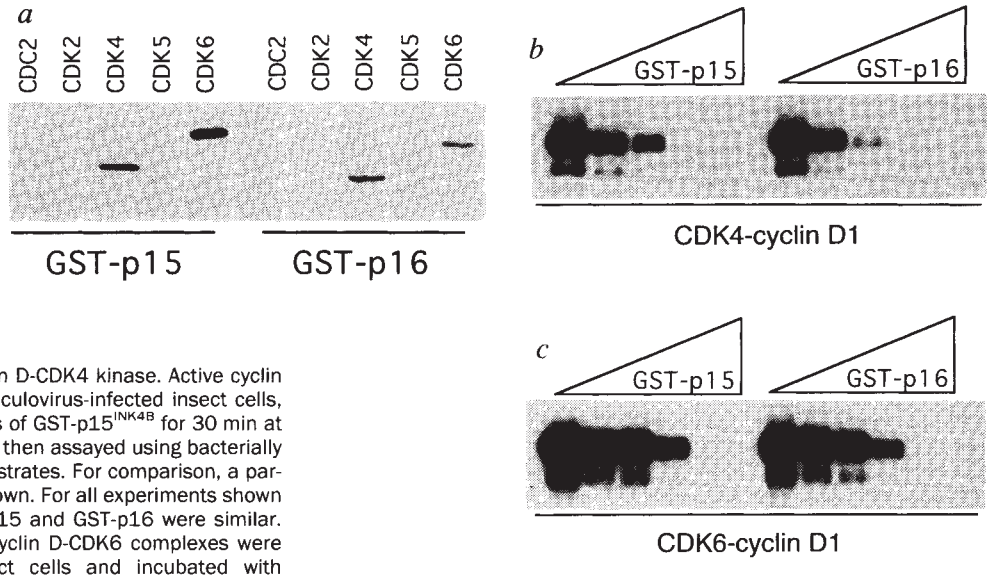

FIG. 2 Specific inhibition of CDK4 and CDK6 by p15. *a*, Binding of CDK4 and CDK6 by p15. A fusion protein consisting of p15 and glutathione-S-transferase (GST-p15) was purified from bacteria and mixed with equal quantities of *in vitro* translated, ^{35}S-labelled CDC2, CDK2, CDK4, CDK5 or CDK6 (as indicated). Bound proteins were recovered on glutathione sepharose and then released by boiling in SDS gel sample buffer. Bound proteins were analysed by electrophoresis in a 17.5% PAGE gel. For comparison, a similar experiment using GST-p16 is also shown. *b*, p15 binding inhibits cyclin D-CDK4 kinase. Active cyclin D-CDK4 kinase, present in lysates of baculovirus-infected insect cells, was incubated with increasing quantities of GST-p15^{INK4B} for 30 min at 30 °C. Cyclin D-CDK4 kinase activity was then assayed using bacterially produced GST-Rb and [γ-^{32}P]ATP as substrates. For comparison, a parallel experiment using GST-p16^{INK4} is shown. For all experiments shown in this figure, quantities of intact GST-p15 and GST-p16 were similar. *c*, p15 inhibits cyclin D-CDK6 kinase. Cyclin D-CDK6 complexes were produced in baculovirus-infected insect cells and incubated with increasing quantities of GST-p15 or GST-p16 (indicated) as described above. Following incubation, the ability of these complexes to catalyse GST-Rb phosphorylation was determined. For *b* and *c*, GST-Rb was recovered on glutathione sepharose and released by boiling in SDS sample buffer before electrophoresis.

METHODS. Preparation of GST-p16 fusion protein from bacteria has been described previously[9]. GST-p15 was prepared identically. For the binding assays *in vitro* translated CDKs were prepared using the TNT-lysate *in vitro* translation kit (Promega) according to the manufacturer's instructions. For the binding assay, GST-p15 or GST-p16 (250 ng) was incubated with *in vitro* translated CDKs for 30 min at 30 °C in 30 µl containing 20 mM Tris, pH 8.0, 10 mM $MgCl_2$, 1 mM EGTA. following incubation, mixtures were diluted to 250 µl in IP buffer (50 mM Tris, pH 8.0, 150 mM NaCl, 0.5% NP-40) and incubated for 1 h with 12.5 µl of glutathione sepharose. Beads were washed four times with 1 ml of IP buffer before release of bound proteins. For kinase assays baculovirus lysates containing active cyclin D-CDK4 were prepared as described previously[9,28]. Lysates containing active cyclin D-CDK6 were prepared identically (the CDK6 baculovirus was a gift of M. Meyerson, MGH). For kinase assays 10 µl of baculoviral lysates were mixed with approximately 0, 10 ng, 20 ng, 50 ng, or 100 ng GST-p15 or GST-p16 and incubated for 30 min at 30 °C in a total volume of 30 µl containing 20 mM Tris, pH 8.0, 10 mM $MgCl_2$, 1 mM EGTA. Following incubation, 0.5 µg GST-Rb and 0.5 µl [γ-^{32}P]ATP (5 µCi, 3000 Ci mmol^{-1}) were added for 10 min at 30 °C. Reactions were stopped by the addition of 250 µl IP buffer and 15 µl glutathione sepharose. After a further hour of incubation at 4 °C, beads were washed four times with IP buffer before release of bound proteins and subsequent electrophoresis.

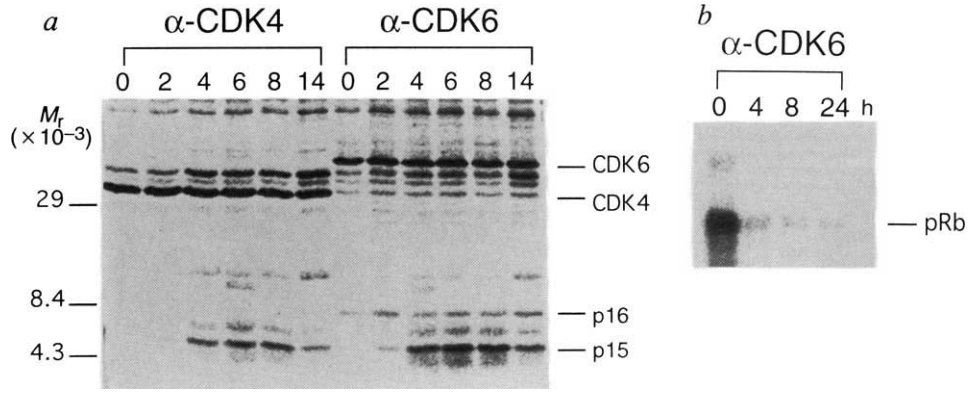

FIG. 3 *a*, Increased association of p15^{INK4B} with CDK4 and CDK6 after TGF-β treatment. Asynchronous HaCaT cells at ~50% confluence were treated with 2 ng ml^{-1} TGF-β for the times indicated. For the last 2 h of TGF-β treatment, cells were labelled with [^{35}S]methionine. Cells were lysed and proteins were immunoprecipitated using either α-CDK4 or α-CDK6 antibodies (as indicated). The positions of p15, p16, CDK4 and CDK6 are marked. The positions of labelled protein molecular weight markers electrophoresed in parallel are also shown. *b*, Inhibition of CDK6 kinase after TGF-β treatment. Asynchronous cells were treated for the indicated times with TGF-β (2 ng ml^{-1}). Cells were lysed in IP buffer (see above) and proteins were recovered by immunoprecipitation with a CDK6 antibody (gift of M. Meyerson). The kinase activity of CDK6 complexes present in the immunoprecipitates was tested using GST-Rb as a substrate[4]. Parallel immunoprecipitates, analysed for protein composition of CDK6 complexes, showed significant accumulation of p15 starting at the 4-h time point (data not shown). The position of the phosphorylated pRB is indicated.

METHODS. HaCaT cells were cultured as described above. TGF-β treatment was initiated by adding TGF-β to existing media to 2 ng ml^{-1}. For cell labelling, medium was changed to DMEM minus methionine (Gibco-BRL) containing 0.2 ng ml^{-1} TGF-β, 10% dialysed FBS and 0.5 mCi ml^{-1} [^{35}S]-methionine/cysteine (trans-label, NEN). Cell lysis and immunoprecipitation were as described above. HaCaT cultures treated with TGF-β in parallel were stained with DAPI and analysed by FACS. For 8 h following TGF-β addition, there was no appreciable change in the percentage of G1 cells. After 14 h, the G1 population began to increase. Arrest of HaCaT cells in G1 (~85% G1 cells) required at least 24 h after treatment of an asynchronous culture. For kinase assays, ^{35}S-labelled, TGF-β-treated cells were lysed in IP buffer (see above). Proteins were recovered using a CDK6-specific antiserum and protein A-sepharose (Pierce). Immunoprecipitates were split for analysis of complex components (not shown) and kinase assays. The beads reserved for the kinase assay were washed three times in IP buffer then twice in kinase buffer (see above). (20 µl) Kinase buffer containing 0.5 µg GST-Rb and 5 µCi [γ^{32}P]ATP were then added to the beads, and the reactions were incubated for 10 min at 30 °C. Reactions were stopped by the addition of 300 µl IP buffer, and protein A-Sepharose was removed by centrifugation. Glutathione sepharose (15 µl) was added to the supernatant to separate GST-Rb from unreacted [γ-^{32}P]ATP. Subsequent processing and analysis were as described in the legend to Fig. 2. To date, using our CDK4 and cyclin D1 antibodies, we have been unable to assay CDK4 kinase from a variety of cell types and thus were not able to examine the effects of TGF-β on the activity of these complexes.

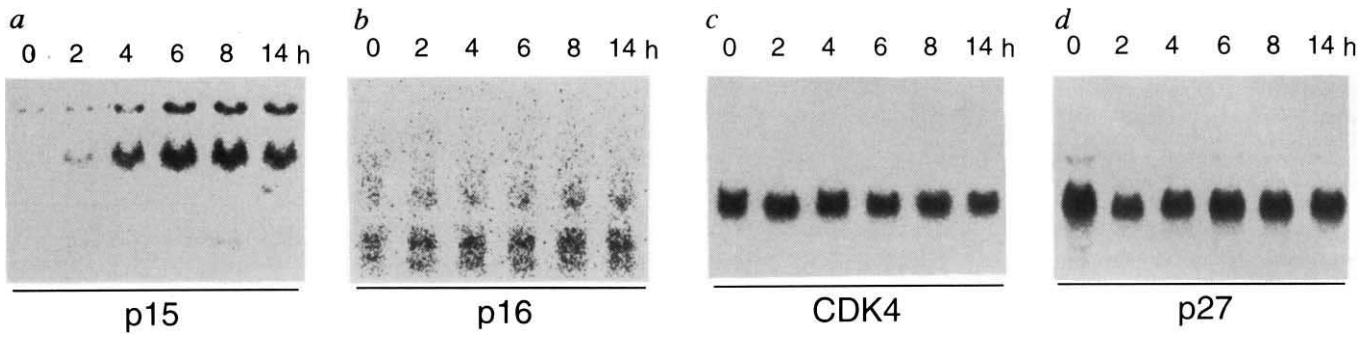

FIG. 4 Induction of p15 mRNA by TGF-β treatment *a*, Asynchronous HaCaT cultures were treated with TGF-β for the indicated times. Total RNA was prepared from treated cells and used for northern blotting with a probe specific for $p15^{INK4B}$, which recognizes three p15 mRNAs of around 0.8, 2.2 and 3.2 kb. *b*, RNAs identical to those used in *a* were probed with a fragment specific for $p16^{INK4}$. *c*, RNA from TGF-β-treated HaCaT cells (see *a*) was probed with a fragment encoding human CDK4. *d*, RNA from TGF-β-treated HaCaT cells was probed with a fragment of $p27^{Kip1}$ cDNA (a gift of H. Zhang, Cold Spring Harbor Laboratory). *e*, Northern signals from panels *a–d* were quantitated on a Fuji BAS2000 phosphorimager and plotted to give a graphical representation of the results. In each case, the amount of transcript detected in the absence of TGF-β is defined as 1.0. Relative increases or decreases in mRNA abundance are plotted with respect to the zero time point.

METHODS. HaCaT cells were treated with TGF-β as described in the legend to Fig. 3. RNA was prepared from treated cultures using RNAZOL B according to the manufacturer's instructions. p15 and p16-specific probes consisted of the first coding exons of these genes and were prepared by PCR. No cross hybridization of probes was evident under the conditions used for these northern blots (hybridization: 200 mM $NaPO_4$, pH 7.0, 1 mM EDTA, 15% formamide, 7% SDS, 0.1% bovine serum albumin at 65 °C; wash: 0.2 × SSC, 65 °C). The CDK4 and $p27^{Kip1}$ probes consisted of the coding sequences of the respective cDNAs. RNA amounts were normalized by mass, and over-probing of the blot shown in *c* with a human actin probe suggested no more than 10% variance in RNA amounts between lanes.

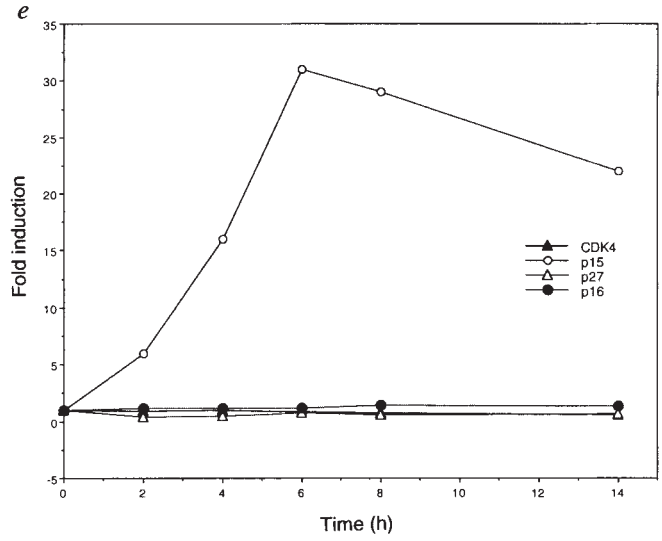

mRNA (Fig. 4*c*, *e*) levels. On the basis of the properties of p15, we would predict that CDK4 overexpression could also render HaCaT cells TGF-β resistant by titrating the p15 CDK4/CDK6 inhibitor. $p27^{Kip1}$, a CDK inhibitor that was purified from TGF-β-arrested cells, has also been proposed as a link between TGF-β and cell cycle control[12–14]. However, in HaCaT cells, TGF-β treatment had no effect on p27 mRNA levels (Fig. 4*d*, *e*). p27 mRNA was also unaffected by similar treatment of Mv1Lu cells[12]. Thus in these cell lines, any contribution that p27 might make to TGF-β-mediated cell cycle arrest would have to occur by regulation at the post-translational level.

Considered together, our results suggest that $p15^{INK4B}$ may function as an effector of TGF-β-mediated cell cycle arrest through inhibition of CDK4 and CDK6 kinases. At present, we cannot distinguish whether p15 acts as the sole mediator of TGF-β-induced arrest in some cells or whether p15 must cooperate with other TGF-β-responsive pathways[1,11–14]. In specific cell types, TGF-β can also induce differentiation[1]. Withdrawal from the cell cycle has been proposed as a component of differentiation, and induction of p15 by TGF-β could contribute to this process.

Cytogenetic abnormalities at 9p21 are common in many types of human tumours, suggesting the presence of a tumour suppressor gene at this locus[15–17]. An inherited cancer syndrome which causes predisposition to melanoma also maps to 9p21 (refs 18–20). $p16^{INK4}$ was initially proposed as a candiate for both of these activities on the basis of analysis of p16 deletions and point mutations in cell lines[10,21]. However, the presence of a second functional member of the p16 family at 9p21 raises the possibility that loss of tumour suppression may involve inactivation of either or both genes. The response of p16 to viral oncoproteins indicates that it may function in intracellular growth regulatory pathways[9,22], and results presented here suggest that p15 may act as an effector of extracellular growth inhibitory signals. Thus, deletions of 9p21 which remove both genes (or other mutations that might inactivate both) could simultaneously negate two major proliferation control pathways. In this regard, the ability of TGF-β to induce growth arrest is reduced or lost in many neoplastically transformed cell lines[1,23–25]. In particular, melanocytes are sensitive to growth inhibition by TGF-β, but many metastatic melanoma cells are TGF-β resistant[26]. □

Received 7 July; accepted 29 July 1994.

1. Massague, J. *A. Rev. Cell Biol.* **6,** 597–641 (1990).
2. Sherr, C. J. *Cell* **73,** 1059–1065 (1993).
3. Bates, S. *et al. Oncogene* **9,** 71–79 (1994).
4. Meyerson, M. & Harlow, E. *Molec. cell. Biol.* **14,** 2077–2086 (1994).
5. Laiho, M., DeCaprio, J. A., Ludlow, J. W., Livingston, D. M. & Massague, J. *Cell* **62,** 175–185 (1990).
6. Pietenpol, J. *et al. Cell* **61,** 777–785 (1990).
7. Boukamp, P. *et al. J. Cell Biol.* **106,** 761–771 (1988).
8. Geng, Y. & Weinberg, R. A. *Proc. natn. Acad. Sci. U.S.A.* **90,** 10315–10319 (1993).
9. Serrano, M., Hannon, G. J. & Beach, D. *Nature* **366,** 704–707 (1993).
10. Kamb, A. *et al. Science* **264,** 436–440 (1994).
11. Ewen, M. E., Sluss, H. K., Whitehouse, L. L. & Livingston, D. M. *Cell* **74,** 1009–1020 (1993).
12. Polyak, K. *et al. Cell* **78,** 59–66 (1994).
13. Toyoshima, H. & Hunter, T. *Cell* **78,** 67–74 (1994).
14. Polyak, K. *et al. Genes Dev.* **8,** 9–22 (1994).
15. Bello, M. J., *et al. Genes Chromosomes Cancer* **9,** 33–41 (1994).
16. Merlo, A., Gabrielson, E., Askin, F. & Sidransky, D. *Cancer Res.* **54,** 640–642 (1994).
17. Cheng, J. Q., Jhanwar, S. C., Lu, Y. Y. & Testa, J. R. *Cancer Res.* **53,** 4761–4763 (1993).
18. Petty, E. M. *et al. Am. J. hum. Genet.* **53,** 96–104 (1993).
19. Fountain, J. E. *et al. Proc. natn. Acad. Sci. U.S.A.* **89,** 10557–10561 (1992).
20. Cannon-Albright, L. A. *et al. Science* **258,** 1148–1152 (1992).
21. Nobori, T. *et al. Nature* **368,** 753–756 (1994).
22. Xiong, Y., Zhang, H. & Beach, D. *Genes Dev.* **7,** 1572–1583 (1993).
23. Moses, H. L. *et al.* in *Cancer Cells* (eds Feramisco, J., Ozanne, B. & Stiles, C.) **3,** 65–71 (1985).
24. Masui, T. *et al. Proc. natn. Acad. Sci. U.S.A.* **83,** 2438–2442 (1986).

25. Manning, A. M., Williams, A. C., Gamie, S. M. & Paraskeva, C. *Oncogene* **6,** 1471–1476 (1991).
26. Rodeck, U. *et al. Cancer Res.* **54,** 575–581 (1994).
27. Hannon, G. J., Demetrick, D. & Beach, D. & Beach, D. *Genes Dev.* **7,** 2378–2391 (1993).
28. Xiong, Y. *et al. Nature* **366,** 701–704 (1993).

ACKNOWLEDGEMENTS. We thank S. Matsumoto and C. Gawel for technical assistance and P. Renna, M. Ockler and J. Duffy for photography and graphics. M. Stampfer (Berkeley), M. Meyerson (MGH), P. Boukamp and N. Fusenig (German Cancer Research Center) provided critical reagents. We are grateful to Hui Zhang for providing baculoviral lysates and for helpful discussions. G.J.H. is a fellow of the Damon Runyon–Walter Winchell Cancer Research Fund. D.B. is an Investigator of the Howard Hughes Medical Institute. This work was supported in part by the NIH.

Location of a folding protein and shape changes in GroEL–GroES complexes imaged by cryo-electron microscopy

Shaoxia Chen*, Alan M. Roseman*, Allison S. Hunter*, Stephen P. Wood*, Steven G. Burston†, Neil A. Ranson†, Anthony R. Clarke† & Helen R. Saibil*

* Department of Crystallography, Birkbeck College London, London WC1E 7HX, UK
† Department of Biochemistry and Centre for Molecular Recognition, University of Bristol, Bristol BS8 1TD, UK

PROTEIN folding mediated by the molecular chaperone GroEL occurs by its binding to non-native polypeptide substrates and is driven by ATP hydrolysis[1]. Both of these processes are influenced by the reversible association of the co-protein, GroES (refs 2–4). GroEL and other chaperonin 60 molecules[5] are large, cylindrical oligomers consisting of two stacked heptameric rings of subunits[6,7]; each ring forms a cage-like structure[8] thought to bind polypeptides in a central cavity[8–10]. Chaperonins play a passive role in folding by binding or sequestering folding proteins to prevent their aggregation[11–13], but they may also actively unfold substrate proteins trapped in misfolded forms, enabling them to assume productive folding conformations[14–16]. Biochemical studies show that GroES improves the efficiency of GroEL function[2,3,17], but the structural basis for this is unknown. Here we report the first direct visualization, by cryo-electron microscopy, of a non-native protein substrate (malate dehydrogenase) bound to the mobile, outer domains at one end of GroEL. Addition of GroES to GroEL in the presence of ATP causes a dramatic hinge opening of about 60°. GroES binds to the equivalent surface of the GroEL outer domains, but on the opposite end of the GroEL oligomer to the protein substrate.

Size-exclusion chromatography of purified GroEL in the presence of ATP releases a significant amount of residually bound protein and peptide to generate an 'emptied' state. Cryo-electron microscope (cryo-EM) side- and end-view projections (Figs 1 and 2*a*, *b*) of this emptied GroEL were aligned and averaged, and a three-dimensional reconstruction was calculated from the averages by backprojecting the seven symmetry-related side views and the end view. Figure 1*c* shows a central section (21 Å thick) of this map. The side projection shows that the overall dimensions of the 14-mer are 140 Å high by 130 Å wide. The end projection is not 7-fold averaged, and demonstrates the strong 7-fold symmetry of the structure. The side-view section (Fig. 2*c*) shows the two major domains of each subunit, with the inner domains forming the interface between top and bottom heptameric rings, and outer domains surrounding a 35–40-Å diameter hole. A three-dimensional surface-contoured view of the structure is shown in Fig. 4*b*.

The stable complex between GroEL and malate dehydrogenase (MDH) was formed by mixing GroEL with a 2.4-fold molar excess of chemically denatured MDH (GroEL 14-mer : MDH monomer) to saturate the available binding sites (see Fig. 2 legend). Figure 2*d–f* shows the cryo-EM images of this binary complex. Comparison with the 'empty' structure reveals a distinct region of additional density at only one end of the oligomer in the side views, and extra density fills the hole seen in the end projection. Difference maps of the end projection and the section are shown in Fig. 2*g* and *h* with the empty GroEL contours superimposed. These maps locate the MDH density in one end cavity of GroEL, between the outer domains and protruding slightly. The visible ligand density (which has been rotationally averaged about the vertical axis in the section view; Fig. 2*h*) occupies a volume roughly similar to that of the 34,000-M_r native subunit (approximately $50 \times 30 \times 35$ Å), but diffuse density may extend into a larger volume. The asymmetric complex is consistent with a spectroscopically determined binding stoichiometry of 1:1 (refs 18, 19, and S.G.B. and A.R.C., unpublished observations), and implies negative cooperativity of ligand binding.

Binding of Mg–ATP to GroEL is sufficient to release some substrate proteins, but others are not released into productive folding forms by ATP unless GroES is also present. To investigate the structural influence of Mg–ATP alone, a set of cryo-EM images of empty GroEL incubated in Mg–ATP were collected and are shown in Fig. 3*a–c*. Compared with GroEL (Fig. 2*c*), GroEL–ATP shows a slight vertical expansion of the oligomer (from 140 to 150 Å) owing to an opening of the outer domains (Fig. 3*a*, *c*). This outer domain displacement differs from that deduced from previous negative stain electron microscopic work[8]. An important factor seems to be the presence of tightly bound substrates in the earlier study, as cryo-EM images of the GroEL–ATP complex made from non-emptied GroEL more closely resemble the previous negative stain findings (not shown). On the basis of the present cryo-EM data, there may be a slight asymmetry in the GroEL–ATP complex. The three-dimensional view of GroEL–ATP in Fig. 4*c* shows the petal-like opening of the outer domains.

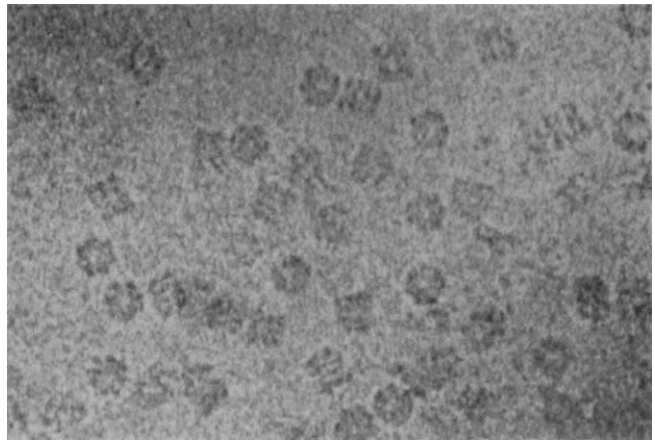

FIG. 1 Unstained, frozen-hydrated GroEL oligomers were imaged in vitreous ice over holes in the carbon support film. The dark regions represent protein density, contrasted against the background of vitreous ice. Two orientations of the oligomers are present: end views, which show the 7-fold symmetry, and side views with four layers of density. METHODS. Solutions containing 1–2 mg ml^{-1} GroEL in 10 mM ammonium acetate and 10 mM Tris buffer pH 7.6 were prepared at room temperature, vitrified by plunging into liquid ethane and imaged at −170 °C. Cryo-EM was done on a JEOL 1200 EX microscope with an Oxford Instruments cryotransfer stage. All images used in the following analysis were recorded with an electron dose ≈10 e Å^{-2} and with a defocus in the range 500–850 nm.